Experimental investigation on heat transfer and friction factor for an inclined spherical ball roughened solar air heater

Ramesh Murmu*, P. Kumar, H. N. Singh

Research Scholar, Mechanical Engineering Department,
NIT Jamshedpur Jharkhand 831014, India

murmunitjsr@gmail.com

ABSTRACT. *The purpose of present investigation is to determine the results of heat transfer and frictional losses for an inclined spherical ball roughened solar air heater. Experimentation was conducted under actual outdoor condition at the test rig designed and fabricated at the terrace of the Mechanical Engineering Department, NIT Jamshedpur, India. To show the effect of ever-changing environmental variables like solar radiation, wind velocity, ambient temperature, etc, on the heat transfer results, the readings were noted for every 15 minutes in the experimental hours 10:00 to 15:00 hours. The present paper deals with the experimental results drafted in the form of rise in Nusselt number (Nu) and friction factor (f) for spherical ball roughened solar air heater (SAH) over those of smooth ones. Flow and roughness geometrical parameters have been varied as relative roughness pitch (p/e) 9-18, relative roughness height (e/D_h) 0.024-0.040, ball's height to diameter ratio (e/d_b) 0.5-2, angle of attack (α) 35˚-75˚ and Reynolds no (Re) 2500-18500. Parametric analysis has also been made and the effects of these parameters on Nu and f characteristics have been shown. This article reveals that maximum augmentation in 'Nu' & 'f' for varying 'p/e', 'e/D_h' & 'e/d_b' and 'α' was respectively found to be of the order of 2.1 to 3.54 times, 1.87 to 3.21 times and 2.89 to 3.27 & 1.74 to 3.56 times for 'Nu' and 0.84 to 1.79 times, 1.46 to 1.91 times, 1.67 to 2.34 times & 1.21 to 2.67 times for 'f' in compared to non-roughened duct. The optimum roughness parameters found under present investigation is $p/e = 15$, $e/D_h = 0.036$, $e/d_b = 1$ and $\alpha = 55$˚. The findings of this research may serve as a criteria to determine thermal and thermohydraulic performance of such roughened solar air heaters and to understand the magnitude of useful heat gain choosing such roughness geometry.*

RÉSUMÉ. *L'objet de la présente enquête est de déterminer les résultats du transfert de chaleur et des pertes par frottement pour un aérotherme solaire à bille sphérique inclinée. Les essais ont été menés dans des conditions extérieures réelles sur le banc d'essai conçu et fabriqué sur la terrasse du département d'ingénierie mécanique de NIT Jamshedpur, en Inde. Afin de montrer l'effet de variables environnementales en constante évolution, telles que le rayonnement solaire, la vitesse du vent, la température ambiante, etc., sur les résultats du transfert de chaleur, les lectures ont été notées toutes les 15 minutes entre 10h00 et 15h00. Cet article traite des résultats expérimentaux rédigés sous la forme d'une augmentation du nombre de Nusselt (Nu) et du coefficient de frottement (f) pour l'aérotherme solaire rugueux à bille sphérique inclinéccce (SAH) par rapport à ceux qui sont lisses. Les paramètres géométriques*

d'écoulement et de rugosité ont été modifiés en fonction de l'espacement de rugosité relatif (p / e) 9-18, hauteur de rugosité relative (e / Dh) 0,024-0,040, rapport hauteur / diamètre de la bille (e / db) 0,5-2, angle d'attaque (α) 35˚-75˚ et Reynolds no (Re) 2500-18500. Une analyse paramétrique a également été réalisée et les effets de ces paramètres sur les caractéristiques de Nu et f ont été montrés. Cet article révèle que l'augmentation maximale de 'Nu' & 'f' pour une variation de 'p / e', 'e / Dh' & 'e / db' et 'α' était respectivement de l'ordre de 2,1 à 3,54 fois 1,87 à 3,21 fois et 2,89 à 3,27 & 1,74 à 3,56 fois pour «Nu» et 0,84 à 1,79 fois, 1,46 à 1,91 fois, 1,67 à 2,34 fois & 1,21 à 2,67 fois pour «f» par rapport à un conduit non rugueux. Les paramètres de rugosité optimaux trouvés dans la recherche actuelle sont p / e = 15, e / Dh = 0,036, e / db = 1 et α = 55˚. Les résultats de cette recherche peuvent servir de critères pour déterminer les performances thermiques et thermohydrauliques de ces aérothermes solaires rugueux et pour comprendre l'ampleur du gain de chaleur utile en choisissant une telle géométrie de rugosité.

KEYWORDS: *solar energy, spherical ball, relative roughness pitch, relative roughness height, Height to diameter ratio, angle of attack.*

MOTS-CLÉS: *energie solaire, bille sphérique, espacement de rugosité relatif, hauteur de rugosité relative, Rapport hauteur sur diamètre, angle d'attaque.*

DOI:10.3166/I2M.17.7-36 © 2018 Lavoisier

1. Introduction

Sun is the ultimate source of most of the sources of energy that as per The United Nations Development Programme in its 2000 World Energy Assessment found that the annual potential of solar energy was 1,575–49,837 exajoules (EJ) which was several times larger than the total world energy consumption, which was 559.8 EJ in 2012. With about 300 clear and sunny days in a year, the calculated solar energy incidence on India's land area is about 5000 trillion KWh per year. The solar energy available in a single year exceeds the possible energy output of all of the fossil fuel energy reserves in India (Muneer *et al.*, 2005). Frequent rise in energy prices & demands have motivated many researchers to search for an alternative for non-renewable sources of energy. Harnessing sun's thermal energy has been an effective idea to use solar energy to serve various energy requirements. Solar thermal technology uses the solar heat energy to heat water or air for applications such as space heating, water heating, and cooling for homes and businesses. Artificially roughened SAH uses solar thermal technology where heat transfer augmentation takes place by destroying laminar sub-layer artificially due to the presence of roughness element on collector's surface. Numerous researchers have investigated different roughness geometry with a common purpose to eliminate/reduce the effects of laminar sub-layer on heat transfer. By doing so, the heat transfer from the absorbing medium and underside fluid can be increased and as a result, the thermal efficiency of roughened solar air heater can be increased.

Han *et al*. (1985) investigated the effect of rib pitch to height ratio, and rib height to equivalent hydraulic diameter on friction factor and heat transfer coefficient for Reynolds number range of 7,000 to 90,000, relative roughness pitch range of 10 to 40, and relative roughness height range of 0.021 to 0.063 and found that the maximum

values of friction factor and the Stanton number occur at a relative roughness pitch of 10. Prasad and Saini (1988) develops an empirical correlation for heat transfer coefficient and friction factor for a solar air heater duct artificially roughened by small diameter wires of various relative roughness heights ranging from 0.020 to 0.033 and relative roughness pitch varying from 10 to 20 for Reynolds numbers range between 5000 to 50,000. The results showed that the average friction factor and Nusselt number increased with increase in relative roughness height. The average Nusselt number of the roughened duct was about 2.10, 2.24 and 2.34 times than that of the smooth duct for relative roughness height of 0.020, 0.027 and 0.033 respectively. The average friction factor of the roughened duct was about 3.08, 3.67, and 4.26 times than that of the smooth duct. The increase in the average Nusselt number and average friction factor for relative roughness pitch of 10, 15 and 20 in the roughened duct was about 2.38, 2.14, 2.01 and 4.25, 3.39, 2.93 times than that of the smooth duct respectively. Lau *et al*. (1991) continued their comparison studies on full and staggered discrete ribs arrays and reported that for a constant pumping power, 60˚ and 45˚discrete ribs enhance the ribbed wall heat transfer by about 5 to 19 percent and 11 to 32 percent respectively compared to the corresponding full ribs case. Saini and Saini (2008) experimentally investigated the effect of arc shaped ribs on 'Nu & f' of rectangular ducts of solar air heaters. Enhancement of 'Nu & f' was reported to be of order 3.6 and 1.75 times respectively over smooth. The correlations for Nusselt number and friction factor were also developed. Layek *et al*. (2006) experimentally investigated the effect of transverse chamfered rib-groove roughness on absorber plate of solar air heater and reported that the roughened surface yields about 3.24 fold and 3.78 fold increase in the 'Nu & f' respectively as compared to that of the smooth surface duct. Ahn (2001) investigated the effects of various roughness shapes namely, square, triangular, circular and semi circular on friction factor and heat transfer in a rectangular duct. They observed that the heat transfer of triangular ribs was the highest caused by the most active interaction between the re-circulating fluid flow in the two ribs and the fluid flow over the ribs. Karwa *et al*. (2002) carried out an experimental investigation on the integral transverse chamfered rib roughened absorber plate and found two-fold increase in the Stanton number and three-fold increase in the friction factor as compare of that of the smooth duct. Mahmood *et al*. (2003) studied 45˚ angled rib turbulators and found that the thermal performance is lower in the ribbed channel than in channel with dimples and/or protrusions mostly because of higher rib formed drag and friction factors. Chang *et al*. (2008) investigated experimentally the effect of V-shaped ribs and deepened scales and found that the heat transfer enhancement ratios were 9.5-13.6 and 9-12.3 with forward and backward flows respectively for laminar flows and 6.8-6.3 and 5.7-4.3 for turbulent flows Ridouane and Campo (2007) investigated computationally the heat transfer and pressure drop of laminar air flow in a parallel-plate channel with transverse hemi-cylindrical cavities and found enhancement in heat transfer by 30 % relative to smooth duct and pressure loss increments by 19 %. Gupta *et al*. (1997; 1993) investigated 90˚ continuous, 60˚ broken ribs and 90˚ saw tooth profiled & established that the mean heat transfer for square channel with 60˚ V-broken ribs are more eminent than that of 90˚saw tooth profiled rib and 90˚ continuous ribs. Chandra *et al*. (2003) carried out investigation of the heat transfer and friction behavior of a square duct with transverse ribs roughness

on one, two, three and four walls of the duct. The flow Reynolds number was varied from 10,000 to 80,000, relative roughness height (e/D_h) of 0.0625 and the relative roughness pitch (p/e) of 8. They found that the heat transfer is enhanced with the increase in number of ribbed walls in the channel from 2.16 for one ribbed wall case to 2.57 for four ribbed wall case at a Reynolds number of 30,000. Momin *et al*. (2002) investigated the heat transfer and friction characteristics of duct roughened with V-shaped rib roughness with relative roughness height range of 0.02 to 0.034, angle of attack range of 30°-90° and Reynolds number in the range of 2,500 to 18,000. Relative roughness pitch was kept constant as 10. The maximum enhancement in the heat transfer and friction factor as a result of providing artificial roughness was observed as 2.30 and 2.83 times of that of smooth duct for an angle of attack of 60°. Naphon (2008) investigated experimentally heat transfer and friction characteristics of two opposite corrugated plates with different corrugated tilt angles of 20˚, 40˚and 60˚ and found that due to the breaking and destabilizing in the thermal boundary zone, the corrugated surface has significant effect on the enhancement of heat transfer and pressure drop. Saini and Saini (1997) used expanded metal mesh as artificial roughness at the absorber plate of solar air heater which gave the maximum enhancement in Nusselt number and friction factor of the order of 4 and 5 respectively, and the maximum enhancement in the thermal efficiency was found in the range of 37% to 57%. Varun *et al*. (2008) experimentally investigated heat transfer and friction characteristics of solar air heater by using a combination of inclined and transverse ribs on the absorber plate of rectangular duct. For (p/e) value of 8, the best thermal performance has been obtained. Correlations for Nusselt number and friction factor were also developed. Wongcharee *et al*. (2011) investigated the effects of different shaped ribs [rectangular, triangular, cylindrical, concave-concave, convex-concave, long convex-short concave and long convex-short concave] on heat transfer and friction factor and found that the cylindrical ribs provided the highest value of thermo-hydraulic performance and minimum enhancement in Nusselt number in case of rectangular ribs Sethi *et al*. (2012) experimentally investigated the effect of artificial roughness on heat transfer and friction characteristics in solar air heater duct which is having dimple shaped elements arranged in angular fashion (arc) The maximum value of Nusselt number has been found corresponding to relative roughness height of 0.036, relative roughness pitch of 10 and arc angle of 60˚. Skullong and Promvonge (2014) performed experimental study on the heat transfer and flow friction characteristics in a solar air heater channel fitted with delta-winglet type vortex generators (DWs). The experimental result reveals that in the first case, the 60° DW-E at R_p=1 provides the highest heat transfer and friction factor while the 30° DW-E at R_p=1 performs overall better than the others. In the second case, the 30° DW-A at b/H=0.5 yields the highest heat transfer and friction factor but the best thermal performance is found at b/H=0.4. Pandey *et al*. (2016) experimental studied on heat transfer and friction factor in rectangular channel with multiple-arc shaped with gaps as roughness element. The maximum increment in Nusselt number (Nu) and friction factor (f) was 5.85 and 4.96 times in comparison to the smooth duct. The maximum enhancement for Nu takes place at Reynolds number (Re) = 21,000, g/e=1, d/x= 0.65, W/w=5, e/D_h= 0.044, p/e = 8 and α/60 = 1. Kumar et al. (2017) has used three sides instead of one side roughened duct & found that augmentation in Nu & f' of three sides over one side

roughened duct was respectively to be 21-86 % and 11-41 %. They also reported augmentation in thermal efficiency of three sides over those of one side roughened duct to be 44-56 % for varying p/e and 39-51 % for varying e/D_h.

The literature reveals that considerable amount of experimental & analytical work has been done to investigate the effect of turbulence promoters on 'Nu & f' characteristics of roughened flow passages. It is this elegance of this method which makes it thermo-hydraulically superior to other methods like use of fins and other substantially large protrusions. Extensive experimentations have been carried out in part, employing artificial roughness viz. transverse rib, angled rib, inclined rib with gap, v-shaped rib, discrete or broken v-shaped rib, discrete v-shaped rib with pieces, w-shaped rib, wedge or chamfered shaped rib, dimpled shaped rib, rib-groove, Multi v-shaped rib and z-shaped rib, for heat transfer enhancement in rectangular ducts. However no study has been reported on SAH roughened with inclined spherical ball of different height and diameter soldered upon collector's face. More improvement can be expected in local heat transfer by using spherical ball roughened SAH, as such geometry can increase the number of secondary flow stream due to variation in angle of attack and geometrical dimension. The present research has been taken up with an objective to conduct experimentation under actual outdoor condition on spherical ball roughened SAH, to determine the optimum roughness parameters, determine the rise in 'Nu & f' for roughened duct over those of non-roughened duct The remainder of this paper is organized as follows: Section 2 introduces the details of experimentation and methodologies adopted for acquiring the requisite objectives, Section 3 describes the results and discussions of present investigation and Section 4 presents conclusions.

2. Investigation methodology

Experimentation is conducted to obtain the experimental values of 'Nu_r & f_r' for the inclined spherical ball roughened collectors. The test rig was fabricated and calibrated properly before taking data for roughened and non-roughened ducts. The test rig had two ducts capable of accommodating roughened and non-roughened ducts simultaneously. The various sets of data recorded from the test rig included: inlet and outlet air temperatures, plate temperatures, pressure drop across the duct and the orifice and solar insolation.

2.1. Test rig

The experimental set-up has been designed and fabricated as per the Hale (1986). Fig. 1 & 2 respectively shows the schematic and actual photograph of experimental set-up. A 5 HP Centrifugal blower with a 3.5 kW Electric motor has been provided in the set-up to suck air from atmosphere through the test sections. The rectangular duct is having dimensions of 2150 mm × 330 mm × 30 mm in which the length of test section is 1200 mm and lengths of entry and exit sections are 650 mm and 300 mm respectively. The aspect ratio (W/H) of the duct is 11. The entry section is made a bell-mouthed shape at the inlet side to avoid loses at the entry. Each test section contains a glass cover of 4 mm thickness at the top and a back plate of 3 mm thick G.I

sheet in the bottom. A Control valve was provided to control the flow in both the ducts. Calibrated orifice meter was installed to measure the flow rate of air through the roughened ducts. A copper constantan thermocouple has been provided at various locations to measure the plate temperatures. A digital pyranometer system was used to measure solar radiation, wind velocity, ambient temperatures.

Fig. 3 & 4 shows the actual and schematic diagram of the inclined spherical ball roughened plate used under present study. Fig. 5 shows the schematic diagram of roughened and non-roughened ducts. Fig. 6 shows the positioning of thermocouples on the absorber plates.

2.2. Roughness parameters range

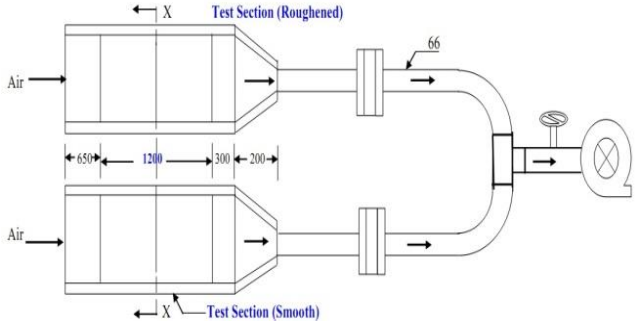

Figure 1. Schematics of test rig

Figure 2. Photograph of test-rig

SAH roughened passage has an L = 1200 mm, H = 30 mm and W = 300mm, the hydraulic diameter, D_h = 54.54 mm. The spherical ball roughness geometry has been

provided under various sets of dimensionless parameters under varying relative roughness pitch (p/e) 9-18, relative roughness height (e/D_h) 0.024-0.040, ball height to diameter ratio (e/d_b) 0.5-2 and relative angle of attack ($\alpha/55$) 35˚-75˚. The flow Reynolds number has been varied from 2500-18500 to generate the best result in terms of 'Nu & f'. Table 1 shows the range of experimental set-up and operating roughness parameters.

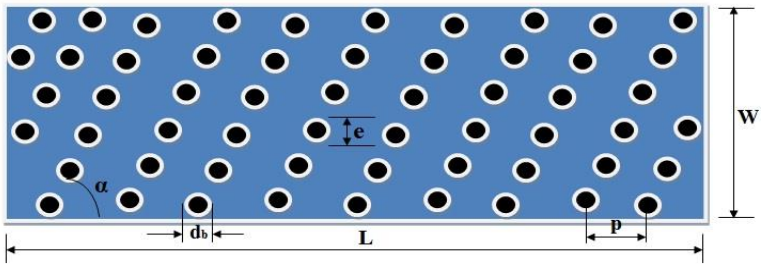

Figure 3. Schematics of spherical ball roughened absorber

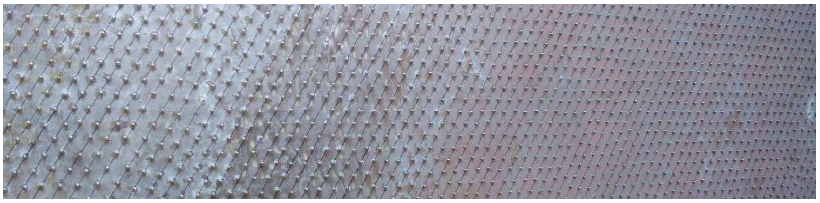

Figure 4. Photograph of spherical ball roughened absorber

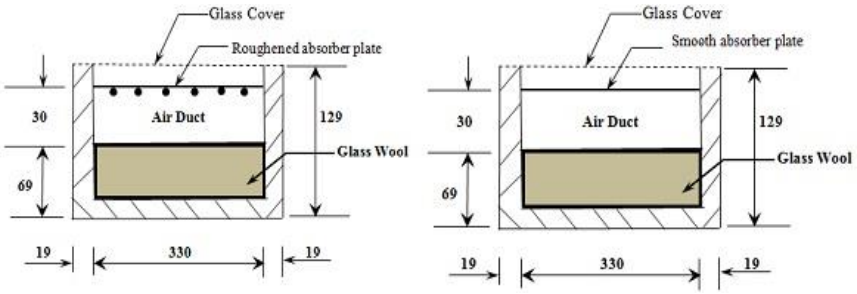

Figure 5. Schematics of roughened and non-roughened ducts

The values/range of geometrical parameters of solar air heater duct, roughness parameters and experimental conditions e.g. mass flow rate, wind velocity, insolation etc. used during experimentation have been given in Table 1.

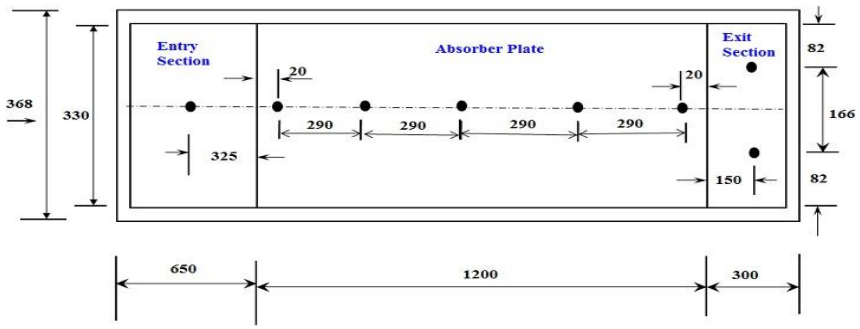

Figure 6. Positioning of thermocouples on absorber

Figure 7. Photograph of pyranometer

Figure 8. Photograph of digital pyranometer system

Table 1. Details of experimental set-up and operating conditions

S. No.		Parameter
1	Duct parameter	Entry length, 650 mm
		Test section length (L), 1200 mm
		Exit length, 300 mm
		Width (W), 330 mm
		Height (H), 30 mm
		Duct aspect ratio (W/H), 11
		Hydraulic diameter (D_h), 54.54 mm
		Glass cover thickness (t_g), 4 mm
		Distance between top glass cover and absorber plate (L_1), 30 mm
2	Roughness parameters	Relative roughness pitch (p/e), 9-18
		Relative roughness height (e/D_h), 0.024-0.040
		Ball height to diameter ratio (e/d_b), 0.5-2
		Angle of attack (α), 35˚-75˚
3	Flow parameters	Mass flow rate (ṁ), 0.0104-0.05126 kg/s
		Reynolds number (Re), 2500-18500
4	Experimen-tal conditions	Ambient temperature (T_a), 21-41, ˚C
		Solar radiation, 674-986, W/m^2
		Wind velocity (W_v), 0.7-3.1, m/s

2.3. Data reduction

The mean temperatures, T_{pm} & T_{fm} are simply the arithmetic mean of the noted values of temperatures at different locations in between the inlet & exit of the test section. Thus:

$$\left(T_{pm}\right)_r = \frac{T_1 + T_2 + \ldots\ldots\ldots + T_6}{6} \tag{1}$$

$$\left(T_{fm}\right)_r = \frac{T_1 + T_6}{2} \tag{2}$$

2.3.1. Mass flow rate measurement

Using the pressure drop measurement across the orifice, the flow rate of air under roughened plate is calculated as:

$$\dot{m} = C_d A_o \left[\frac{2\rho \Delta p_o}{1-\beta^4} \right]^{0.5} \tag{3}$$

2.3.2. Friction factor

The 'f' value is calculated using pressure drop $(\Delta p)_d$, across test section length, L of 1200 mm and the mass flow rate, $\dot{m}$ as**:**

$$f = \frac{\left(\triangle p\right)_d D_h}{2\rho L v_d^{\ 2}} \tag{4}$$

where, D_h: hydraulic diameter for the duct and is evaluated as:

$$D_h = \frac{4WH}{\left[2(W+H)\right]} \tag{5}$$

and, v_d is the flow velocity of air flowing inside the roughened duct.

2.3.3. Reynolds number

The 'Re' is calculated using:

$$\mathrm{Re} = \frac{v_d D_h}{\upsilon} \tag{6}$$

2.3.4. Heat transfer coefficient

Useful heat gain of air is given by:

$$Q_u = \dot{m} C_p \left(T_6 - T_1\right) \tag{7}$$

The heat transfer coefficient for the heated test section has been calculated from:

$$h = \frac{Q_u}{A_p \left(T_{pm} - T_{fm}\right)} \tag{8}$$

where, A_p is the heat transfer area, assumed corresponding one side roughened plate area.

2.3.5. Nusselt number

The heat transfer coefficient is used to determine the 'Nu' and is determined as:

$$Nu = \frac{hD_h}{k} \tag{9}$$

where, 'k': thermal conductivity of the air

2.4. Validation of experimental data

Alongside roughened ducts, data were also recorded for non-roughened duct for validating the experimental set-up. The data of 'Nu_s & f_s' obtained from experimentation have been compared with those of data obtained from the correlation of 'Nu_s & f_s' as per Dittus-Boelter equation and modified Blasius equation respectively.

Nu_s for non-roughened surface as per Dittus-Boelter equation is given by:

$$Nu_s = 0.023\,\mathrm{Re}^{0.8}\,\mathrm{Pr}^{0.4} \tag{10}$$

f_s for non-roughened surface as per modified Blasius equation is given by:

$$f_s = 0.085\,\mathrm{Re}^{-0.25} \tag{11}$$

The data for 'Nu_s & f_s' of non-roughened ducts so obtained from experimentation and the correlations suggested above compared well with a mean deviation in experimental & estimated values of 'Nu_s & f_s' as±3.5% for 'Nu_s'&±4.4% for 'f_s'.

Fig. 9 (a&b) indicates the comparison of experimental values 'Nu_s & f_s' with 'Nu_s' & 'f_s' obtained from the correlations above.

2.5. Uncertainty analysis

Table 2. Uncertainties in measurement of various parameters

S.No.	Name of parameter	Uncertainty range (%)
1.	Area of absorber plate (A_p)	0.07
2.	Cross sectional area of air flow duct (A)	0.16
3.	Area of orifice meter (A_o)	0.21
4.	Hydraulic diameter	0.23
5.	Density	0.106
6.	Mass flow rate	0.84
7.	Velocity of air through test section	0.86
8.	Reynolds Number (Re)	0.9
9.	Heat transfer co-efficient	3.724
10.	Nusselt number (Nu)	4.167
11.	Friction factor (f)	4.389
12.	Useful heat gain	3.14

Based on the method of Kline and Mcclintock (1953) of the uncertainties associated with various parameters, the uncertainties have been discussed and the elaborated form is given in Appendix-A. Uncertainties values of various parameters are given in Table 2.

3. Heat transfer and friction characteristics

Under present experimental studies, effects of spherical ball roughness element parameters such as 'p/e', 'e/D_h', 'e/d_b' & 'α' on 'Nu_r' & 'f_r' has been studied exhaustively and presented as rise in 'Nu_r' & 'f_r' with mass flow rate of air (Reynolds number). To see the effects of these roughness parameters, 'Nu_r' & 'f_r' is plotted against these parameters at some selected values of Reynolds number.

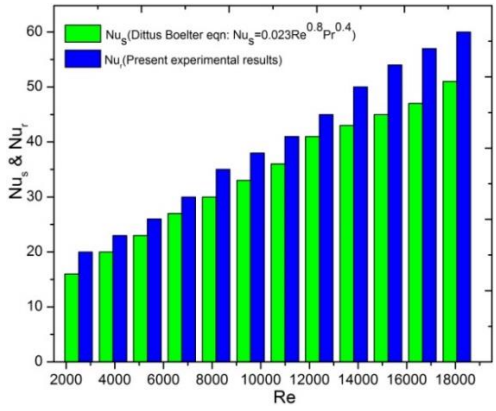

(a) Nu_s

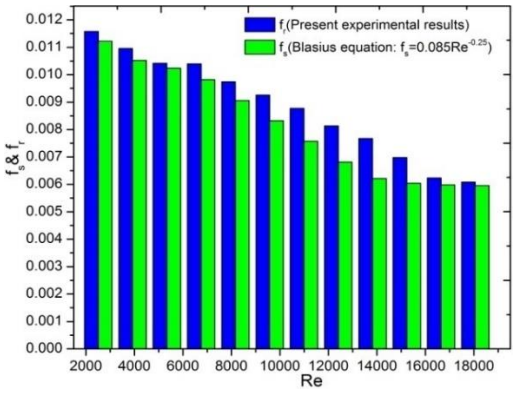

(b) f_s

Figure 9. Comparison b/w experimental and calculated values of 'Nu' & 'f' for one side concave dimple roughened SAH

3.1. Heat transfer and friction factor results

Fig. 10 shows the variation of 'Nu_r' as a function of 'p/e' & 'Re' for fixed 'e/D_h'=0.036, 'e/d_b'=1 & 'α'=55˚. To visualize the effects of 'p/e' on 'Nu_r', the Nusselts number values have been plotted against respective values of 'p/e' at some selected Reynolds number as depicted in Fig. 11. The maximum & minimum value for 'Nu_r' is obtained at 'p/e' of 15 & 9 respectively for the entire values of 'Re' investigated. Likewise, Fig. 12 shows the variation of 'Nu_r' as a function of 'e/D_h' & 'Re' for fixed 'p/e'=12, 'e/d_b'=1 & 'α'=55˚. To visualize the effects of 'e/D_h' on 'Nu_r', the Nusselts number values have been plotted against respective values of 'e/D_h' at some selected Reynolds number as depicted in Fig. 13. The maximum & minimum value for 'Nu_r' is obtained at 'e/D_h' of 0.036 & 0.024 respectively for the entire values of 'Re' investigated. Fig 14 shows the variation of 'Nu_r' as a function of 'e/d_b' & 'Re' for fixed 'e/D_h'=0.036, 'p/e'=12 & 'α'=55˚. To visualize the effects of 'e/d_b' on 'Nu_r', the Nusselts number values have been plotted against respective values of 'e/d_b' at some selected Reynolds number as depicted in Fig. 15. The maximum & minimum value for 'Nu_r' is obtained at 'e/d_b' of 1 & 2 respectively for the entire values of 'Re' investigated. Likewise, Fig. 16 shows the variation of 'Nu_r' as a function of 'α' & 'Re' for fixed 'p/e'=12, 'e/d_b'=1 & 'e/D_h'=0.036. To visualize the effects of 'α' on 'Nu_r', the Nusselts number values have been plotted against respective values of 'α' at some selected Reynolds number as depicted in Fig. 16. The maximum & minimum value for 'Nu_r' is obtained at 'α' of 55˚ & 35˚ respectively for the entire values of 'Re' investigated. It was found that the maximum augmentation in 'Nu' for varying 'p/e', 'e/D_h' & 'e/d_b' and 'α' was respectively found to be of the order of 2.1 to 3.54 times, 1.87 to 3.21 times, 2.89 to 3.27 & 1.74 to 3.56 times with compared to non-roughened duct.

Fig. 18 shows variation of 'f_r' as a function of 'p/e' & 'Re' for fixed 'e/D_h'=0.036, 'e/d_b'=1 & 'α'=55˚. To visualize the effects of 'p/e' on 'f_r', the friction factor values have been plotted against respective values of 'p/e' at some selected Reynolds number as depicted in Fig. 19.

The maximum & minimum value for 'f_r' is obtained at 'p/e' of 9 & 18 respectively for the entire values of 'Re' investigated. Likewise, Fig. 20 shows the variation of 'f_r' as a function of 'e/D_h' & 'Re' for fixed 'p/e'=12, 'e/d_b'=1 & 'α'=55˚. To visualize the effects of 'e/D_h' on 'f_r', the friction factor values have been plotted against respective values of 'e/D_h' at some selected Reynolds number as depicted in Fig. 21. The maximum & minimum value for 'Nu_r' is obtained at 'e/D_h' of 0.040 & 0.024 respectively for the entire values of 'Re' investigated. Fig 22 *shows the* variation of 'f_r' as a function of 'e/d_b' & 'Re' for fixed 'e/D_h'=0.036, 'p/e'=12 & 'α'=55˚. To visualize the effects of 'e/d_b' on 'f_r', the friction factor values have been plotted against respective values of 'e/d_b' at some selected Reynolds number as depicted in Fig. 23. The maximum & minimum value for 'f_r' is obtained at 'e/d_b' of 1 & 2 respectively for the entire values of 'Re' investigated. Likewise, Fig. 24 shows the variation of 'f_r' as a function of 'α' & 'Re' for fixed 'p/e'=12, 'e/d_b'=1 & 'e/D_h'=0.036. To visualize the effects of 'α' on 'f_r', the friction factor values have been plotted against respective values of 'α' at some selected Reynolds number as depicted in Fig.

25. The maximum & minimum value for 'Nu_r' is obtained at 'α' of 55° & 35° respectively for the entire values of 'Re' investigated. It was found that the maximum augmentation in 'f_r' for varying 'p/e', 'e/D_h', 'e/d_b' and 'α' was respectively found to be of the order of 0.84 to 1.79 times, 1.46 to 1.91 times, 1.67 to 2.34 times & 1.21 to 2.67 times compared to non-roughened duct.

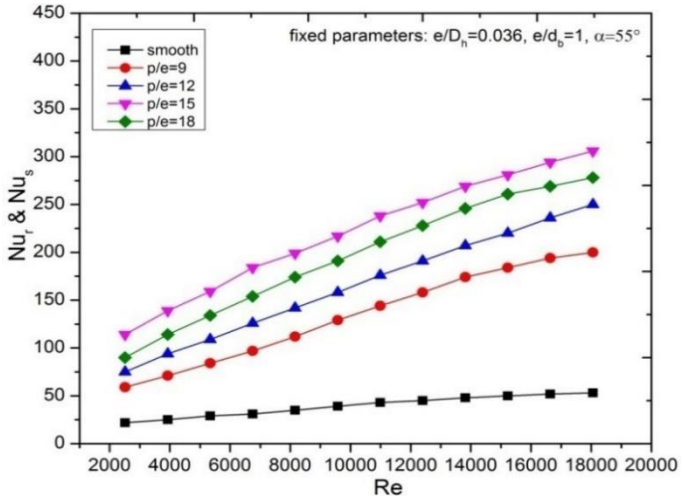

Figure 10. Variation in 'Nu' with 'Re'for different 'p/e' & for fixed 'e/D_h'=0.036, 'e/d_b'=1 & 'α'=55°

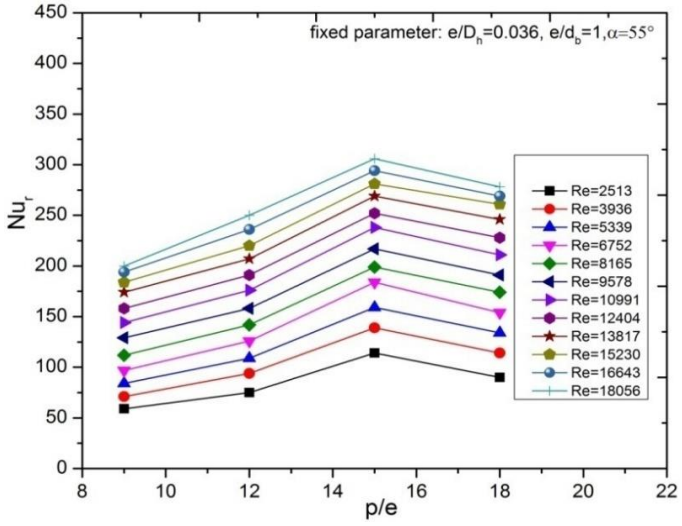

Figure 11. Variation of Nusselt number with 'p/e' for different values of Reynolds Number and for fixed 'e/D_h'=0.036, 'e/d_b'=1 & 'α'=55°

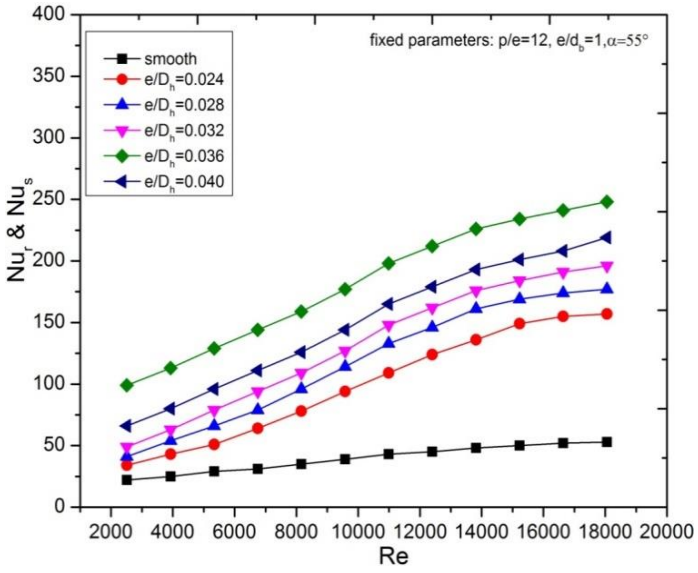

Figure 12. Variation in 'Nu' with 'Re'for different 'e/D_h' & for fixed 'p/e'=12, 'e/d_b'=1 & 'α'=55˚

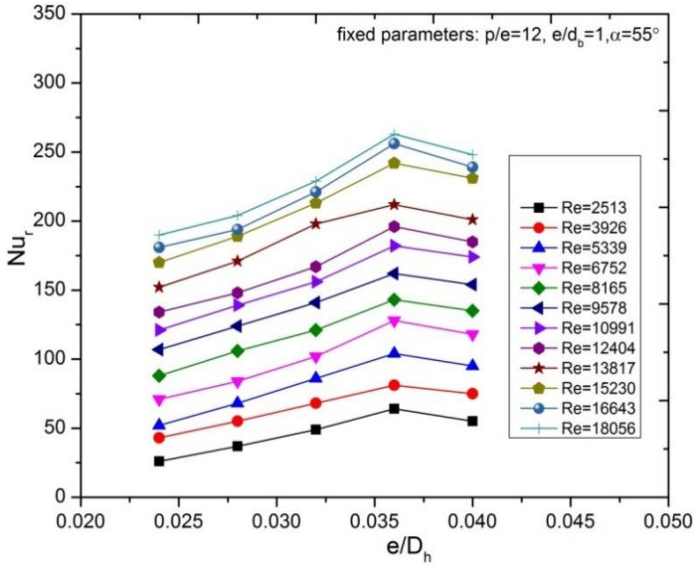

Figure 13. Variation of Nusselt number with 'e/D_h' for different values of Reynolds Number and for fixed 'p/e'=12, 'e/d_b'=1 & 'α'=55˚

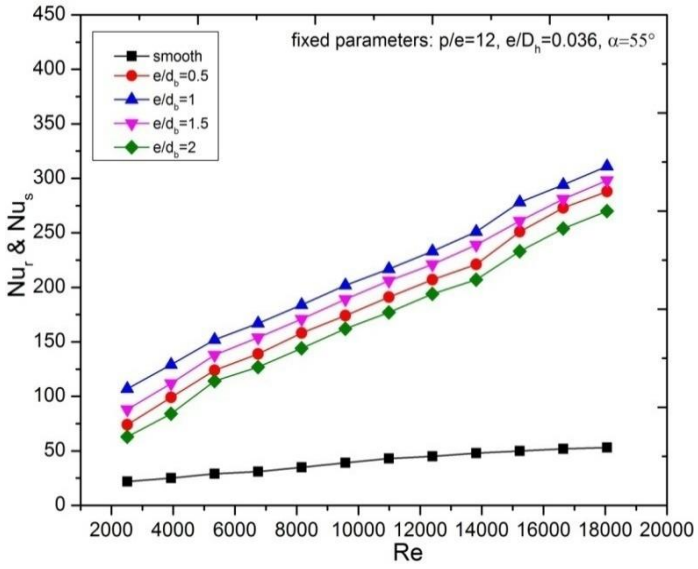

Figure 14. Variation in 'Nu' with 'Re'for different 'e/d_b' & for fixed 'p/e'=12, 'e/D_h'=0.036 & 'α'=55°

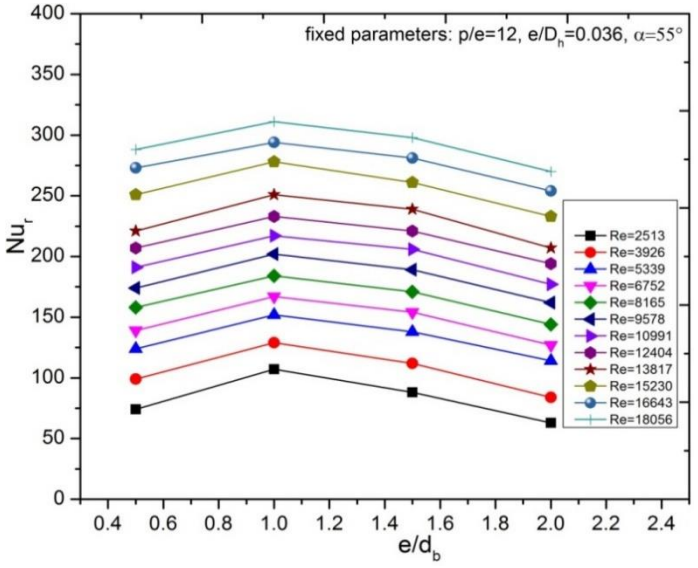

Figure 15. Variation of Nusselt number with 'e/d_b' for different values of Reynolds Number and for fixed 'p/e'=12, 'e/D_h' =0.036 & 'α'=55°

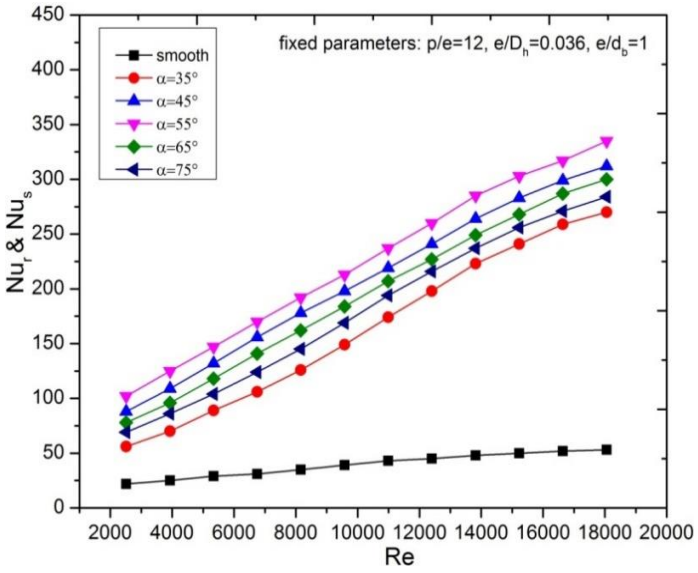

Figure 16. Variation in 'Nu' with 'Re'for different 'α' & for fixed 'p/e'=12, 'e/D_h'=0.036 & 'e/d_b'=1

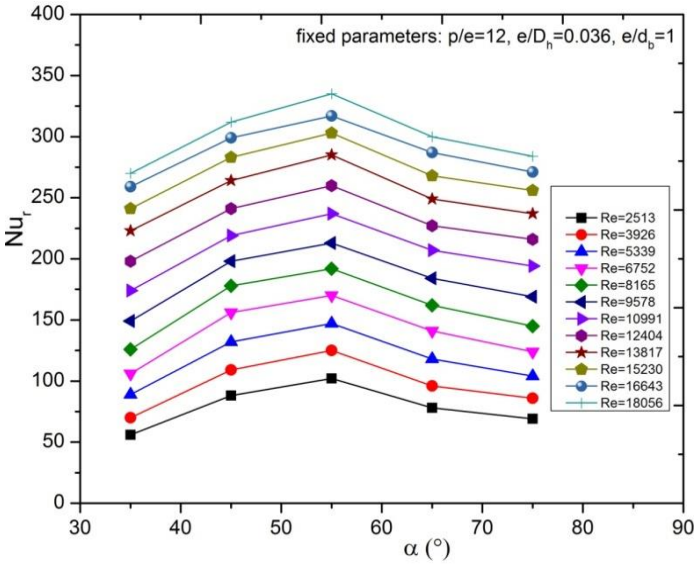

Figure 17. Variation of Nusselt number with 'α' for different values of Reynolds Number and for fixed 'p/e'=12, 'e/D_h' =0.036 & 'e/d_b'=1

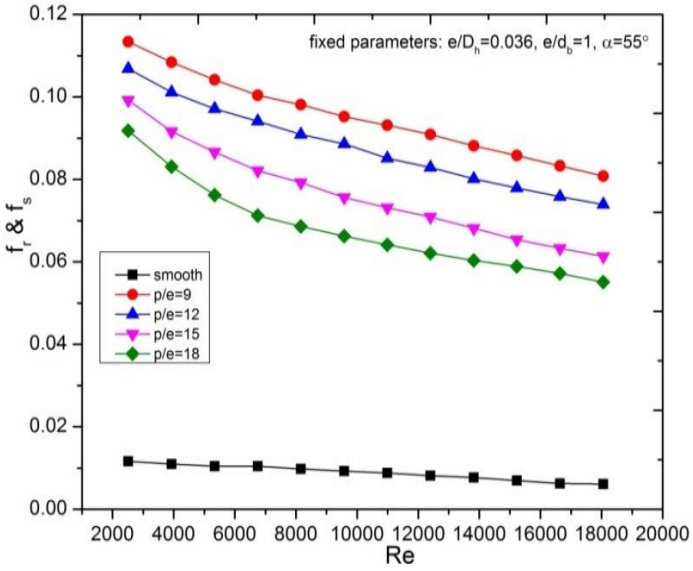

Figure 18. Variation in 'f_r' with 'Re' for different 'p/e' & for fixed 'e/D_h'=0.036, 'e/d_b'=1 & 'α'=55°

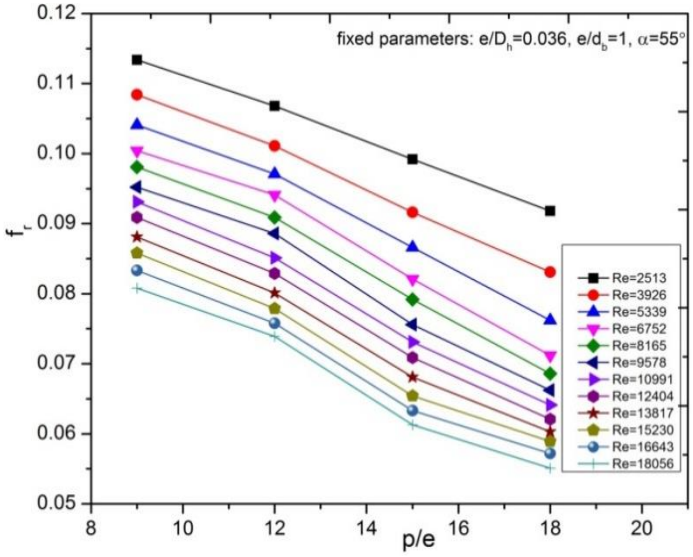

Figure 19. Variation of friction factor with 'p/e' for different values of Reynolds Number and for fixed 'e/D_h'=0.036, 'e/d_b'=1 & 'α'=55°

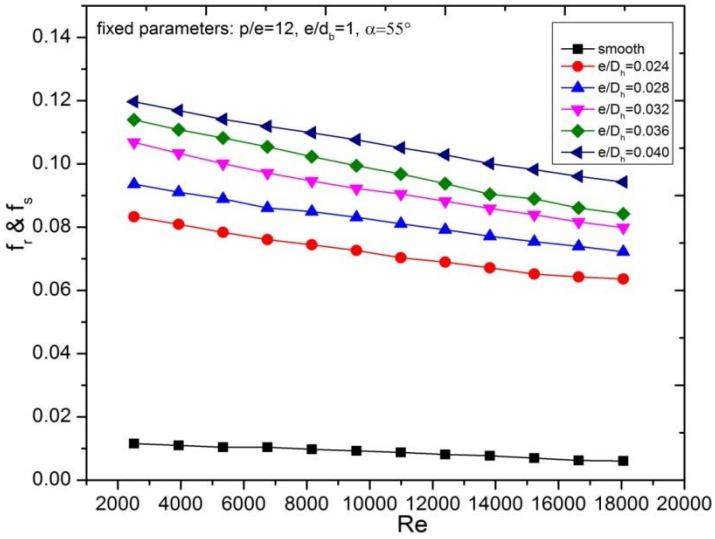

Figure 20. Variation in 'f' with 'Re'for different 'e/D_h' & for fixed 'p/e'=12, 'e/d_b'=1 & 'α'=55˚

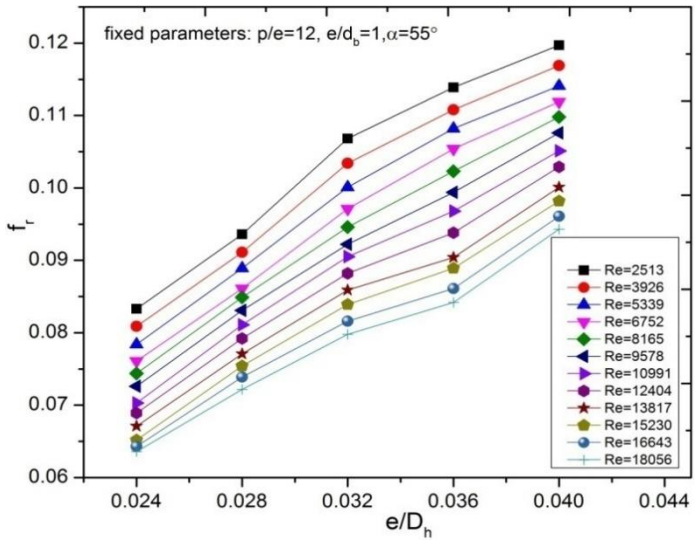

Figure 21. Variation of friction factor with 'e/D_h' for different values of Reynolds Number and for fixed 'p/e'=12, 'e/d_b'=1 & 'α'=55˚

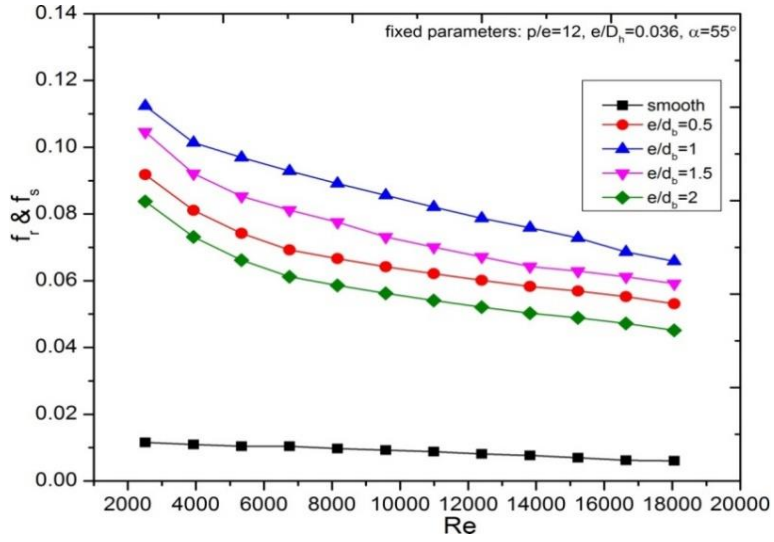

Figure 22. Variation in 'f' with 'Re' for different 'e/d_b' & for fixed 'p/e'=12, 'e/D_h'=0.036 & 'α'=55°

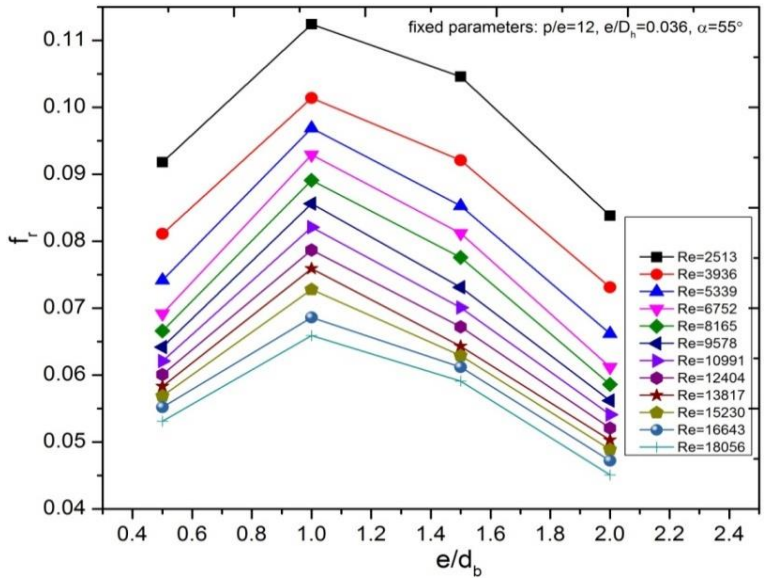

Figure 23. Variation of friction factor with 'e/d_b' for different values of Reynolds Number and for fixed 'p/e'=12, 'e/D_h' =0.036 & 'α'=55°

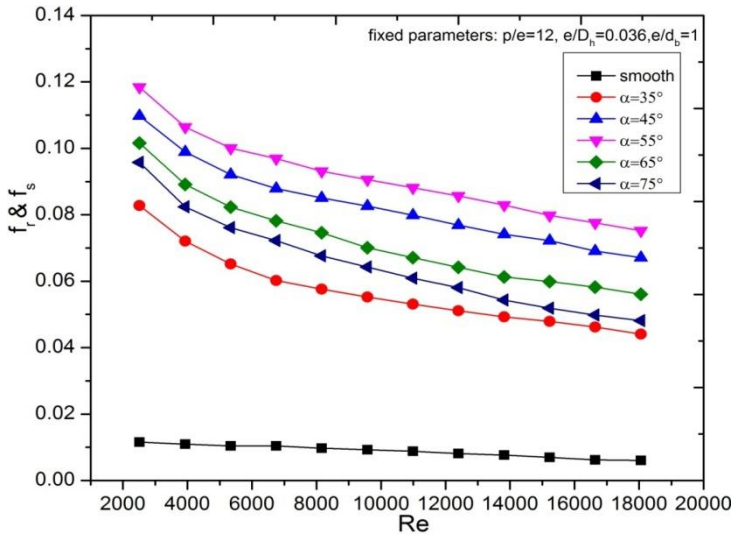

Figure 24. Variation in 'f' with 'Re'for different 'α' & for fixed 'p/e'=12, 'e/D_h'=0.036 & 'e/d_b'=1

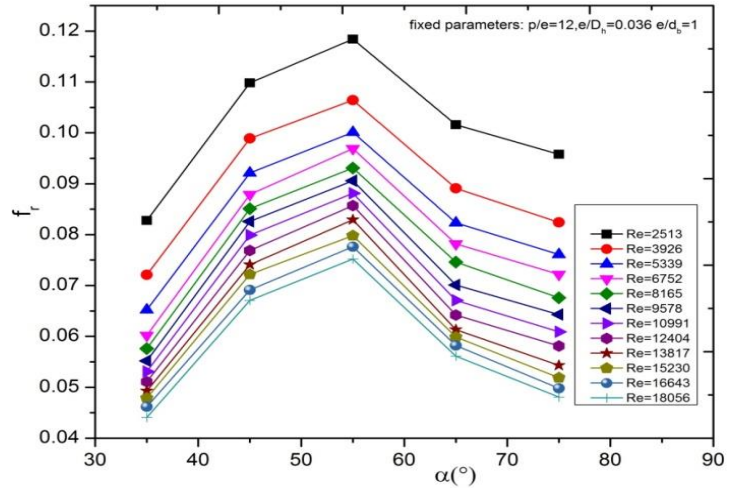

Figure 25. Variation of friction factor with 'α' for different values of Reynolds Number and for fixed 'p/e'=12, 'e/D_h' =0.036 & 'e/d_b'=1

It is clearly evident from this study that heat transfer is a very strong function of flow and geometrical parameters of roughness geometry. Varying the distances between balls exhibited heat transfer augmentation only up to certain values beyond

which any further increament in pitch value resulted in heat transfer decrement. The inclination of spherical ball arrangement also shows that maximum heat transfer occurs at an angle of attack of 55˚. Hence it can be said that heat transfer and fluid flow characteristics of inclined spherical have been investigated of solar air heaters with roughened ducts by providing concave dimple shape geometry on one and three sides of the absorber plates.

4. CONCLUSIONS

An extensive experimental study has been carried out to generate experimental data for heat transfer and pressure drop characteristics in the range of system and operating parameters i.e. relative roughness pitch, (p/e), relative roughness height, (e/D_h), ball height to diameter ratio, (e/d_b), angle of attack (α) and flow Reynolds number (Re).

An elaborative experimental investigation has been carried out under actual outdoor conditions to test the spherical ball roughened SAH and parametric impact on heat transfer and friction characteristics. The results have been shown in the form of rise in 'Nu_r' & 'f_r' for roughened duct over those of non-roughened ones. Experimental data have been used to derive a statistical correlation for 'Nu_r & f_r' in terms of variable parameters. The following conclusions can be drawn from the present study:

1. 'Nu_r' & 'f_r' varied as 'p/e', 'e/D_h', 'e/d_b' & '$\alpha/55$' were varied under the given operating range. In the entire range of 'Re' studied, 'Nu_r' increased as 'p/e' was increased from 9 to 15. On further increasing the value of 'p/e', 'Nu_r' decreased.

2. A similar trend has been found in 'Nu_r' with the variation in 'e/D_h'. 'Nu_r' increased as the 'e/D_h' was increased from 0.024 to 0.036, beyond this, Nusselt number started decreasing with increase in e/D_h value.

3. An increase in ball height to diameter ratio 'e/d_b' resulted in an increase in Nu_r from 0.5 to 1. Upon increasing e/d_b from 1 to 2, it was found 'Nu_r' value was less than so obtained at e/d value of 1.

4. Angle of attack '$\alpha/55$' affected the heat transfer rise as the value of 'Nu_r' increased as angle of attack was increased from 35˚ to 55˚. On further increament in angle of attack value, the 'Nu_r' started decreasing such that the maximum and minimum value of Nu_r was obtained at an angle of attack of 55˚ & 75˚ respectively.

5. The enhancement of 'Nu_r' due to provision of spherical ball on collector's surface was found to be strongly associated with roughness & flow parameters. The maximum augmentation in 'Nu_r' for varying 'p/e', 'e/D_h', 'e/d_b' and '$\alpha/55$' was respectively found to be of the order of 2.1 to 3.54 times, 1.87 to 3.21 times, 2.89 to 3.27 & 1.74 to 3.56 times compared to non-roughened duct. The optimum roughness parameters found under present investigation is 'p/e' = 15, 'e/D_h' = 0.036, 'e/d_b' = 1 and $\alpha = 55$˚.

6. Augmentation in Nu_r is achieved alongwith friction factor rise across the roughened ducts. Friction has been found to decrease monotonously as the 'p/e' was increased from 9 to 18.
7. With the variation of 'e/D_h' from 0.024 to 0.04, the values of 'f_r' increased monotonously with variation in flow and other roughness parameters.
8. As 'e/d_b' was varied from 0.5 to 1, the values of friction factor increased and as the 'e/d_b' values were varied from 1 to 2, the values of friction factor decreased for the entire 'Re' range investigated.
9. The 'f_r' increased as the angle of attack 'α' was increased from 35˚ to 55˚. For further increament in angle of attack from 55˚ to 75˚, 'f_r' decreased.
10. The maximum augmentation in 'f_r' for varying 'p/e', 'e/D_h', 'e/d_b' and 'α' was respectively found to be of the order of 0.84 to 1.79 times, 1.46 to 1.91 times, 1.67 to 2.34 times & 1.21 to 2.67 times compared to non-roughened duct.

References

Ahn S. W. (2001). The effects of roughness types on friction factors and heat transfer in roughened rectangular duct. *International Communications in Heat and Mass Transfer*, Vol. 28, No. 7, pp. 933-942.

Bhagoria J. L., Saini J. S., Solanki S. C. (2002). Heat transfer coefficient and friction factor correlation for the transitional flow regime in rib-roughened rectangular duct. *Renewable Energy*, Vol. 25, No. 3, pp. 341-369. https://doi.org/10.1016/S0960-1481(01)00057-X

Chandra P. R., Alexander C. R., Han J. C. (2003). Heat transfer and friction behaviors in rectangular channel with varying number of ribbed walls. *International Journal of Heat Mass Transfer*, Vol. 46, No. 3, pp. 481-495. https://doi.org/10.1016/S0017-9310(02)00297-1

Chang S. W., Liou T. M., Chiang K. F., Hong G. F. (2008). Heat transfer and pressure drop in rectangular channel with compound roughness of V-shaped ribs and deepened scales. *International Journal of Heat Mass Transfer*, Vol. 51, No. 3-4, pp. 457-468. https://doi.org/10.1016/j.ijheatmasstransfer.2007.05.010

Gupta D., Solanki S. C., Saini J. S. (1993). Heat and fluid flow in rectangular solar air heater ducts having transverse rib roughness on absorber plate. *Solar Energy*, Vol. 51, pp. 31-37. https://doi.org/10.1016/0038-092X(93)90039-Q

Gupta D., Solanki S. C., Saini J. S. (1997). Thermohydraulic performance of solar air heaters with roughened absorber plates. *Solar Energy*, Vol. 61, No. 1, pp. 33–42. https://doi.org/10.1016/S0038-092X(97)00005-4

Hale S. J. B. (1986). Methods of testing to determine the thermal performance of solar collectors. *American Society of Heating, Refrigerating and Air-conditioning Engineers.*

Han, J. C., Park, J. S. and Lei, C. K., 1985, Heat transfer enhancement in channel with turbulence promoters. *Journal Engineering for Gas Turbine and Power*, Vol. 107, No. 3, pp. 628-635. https://doi.org/10.1115/1.3239782

Jaurer A. R., Saini J. S., Gandhi B. K. (2006). Heat transfer coefficient and friction characteristics of rectangular solar air heater duct using rib-grooved artificial roughness. *Solar Energy*, Vol. 80, No. 8, pp. 895-907. https://doi.org/10.1016/j.solener.2005.08.006

Kline S. J., Mcclintock F. A. (1953). Describing uncertainties in single sample experiments. *Mechanical Engineering*, Vol. 75, pp. 3–8.

Kumar V., Prasad L. (2017). Experimental investigation on heat transfer and fluid flow of air flowing under three sides concave dimple roughened duct. *International Journal of Mechanical Engineering and Technology (IJMET)*, Vol. 8, No. 11, pp. 1083–1094.

Kumar V., Prasad L. (2017). Thermal performance investigation of one and three sides concave dimple roughened solar air heaters. *International Journal of Mechanical Engineering and Technology (IJMET)*, Vol. 8, No. 12, pp. 31–45.

Lau S. C., McMillan R. D., Han J. C. (1991). Turbulent heat transfer and friction in a square channel with discrete rib tabulators. *Heat Transfer*, Vol. 113, No. 3, pp. 360-366. https://doi.org/10.1115/1.2927884

Mahmood G. I., Ligrani P. M., Chen K. (2003). Variable property and temperature ratio effects on Nusselts number in a rectangular channel with 45˚ angled rib turbulators. *Journal of Heat Transfer*, Vol. 125, No. 5, pp. 769-778. https://doi.org/10.1115/1.1589503

Momin A. M. E., Saini J. S., Solanki S. C. (2002). Heat transfer and friction in solar air heater duct with V-shaped rib roughness on absorber plate. *International Journal of Heat and Mass Transfer*, Vol. 45, No. 16, pp. 3383-3396. https://doi.org/10.1016/S0017-9310(02)00046-7

Muneer T., Asif M., Munawwar S. (2005). Sustainable production of solar electricity with particular reference to the Indian economy. *Renewable and Sustainable Energy Reviews*, Vol. 9, No. 5, pp. 444-473. https://doi.org/10.1016/j.rser.2004.03.004

Naphon P. (2008). Effect of corrugated plates in an in-phase arrangement on the heat transfer and flow developments. *International Journal of Heat Mass Transfer*, Vol. 51, No. 15-16, pp. 3963-3971. https://doi.org/10.1016/j.ijheatmasstransfer.2007.11.050

Pandey N. K., Bajpai V. K., Varun. (2016). Experimental investigation of heat transfer augmentation using multiple arcs with gap on absorber plate of solar air heater. *Solar Energy*, Vol. 134, pp. 314–326. https://doi.org/10.1016/j.solener.2016.05.007

Prasad B. N., Saini J. S. (1988). Effect of artificial roughness on heat transfer and friction factor in a solar air heater. *Solar Energy*, Vol. 41, No. 6, pp. 555–560. https://doi.org/10.1016/0038-092X(88)90058-8

Ridouane E. I. H., Campo A. (2007). Heat transfer and pressure drop characteristics of laminar air flows moving in a parallel-plate channel with transverse hemi-cylindrical cavities. *International Journal of Heat and Mass Transfer*, Vol. 50, No. 19-20, pp. 3913-3924. https://doi.org/10.1016/j.ijheatmasstransfer.2007.02.004

Saini R. P., Saini J. S. (1997). Heat transfer and friction factor correlations for artificially roughened ducts with expanded metal mesh as roughness element. *International Journal of Heat and Mass Transfer*, Vol. 40, No. 4, pp. 973-986. https://doi.org/10.1016/0017-9310(96)00019-1

Saini S. K., Saini R. P. (2008). Development of correlations for Nusselts number and friction factor for solar air heater with roughened duct having arc-shaped wire as artificial roughness.

Solar Energy, Vol. 82, No. 12, pp. 1118-1130. https://doi.org/10.1016/j.solener.2008.05.010

Sethi M., Varun, Thakur, N. S. (2012). Correlations for solar air heater duct with dimpled shape roughness elements on absorber plate. *Solar Energy*, Vol. 86, No. 9, pp. 2852–2861. https://doi.org/10.1016/j.solener.2012.06.024

Skullong S., Promvonge P. (2014). Experimental Investigation on Turbulent Convection in Solar Air Heater Channel Fitted with Delta Winglet Vortex Generator. Chinese Journal of Chemical Engineering, Vol. 22, No. 1, pp. 1-10. https://doi.org/10.1016/S1004-9541(14)60030-6

Varun, Saini R. P., Singal S. K. (2008). Investigation on thermal performance of solar air heaters having roughness elements as a combination of inclined and transverse ribs on the absorber plate. *Renewable Energy*, Vol. 33, No. 6, pp. 1398-1405. https://doi.org/10.1016/j.renene.2007.07.013

Wongcharee K., Changcharoen W., Eiamsa-ard S. (2011). Numerical investigation of flow friction and heat transfer in a channel with various shaped ribs mounted on two opposite ribbed walls. *International Journal of Chemical Reactor Engineering*, Vol. 9, No. 1, pp. 1-21. https://doi.org/10.1515/1542-6580.2560

Nomenclatures

Parameters	Symbol	Unit
Surface area of absorber plate	A_p	m^2
Area of orifice of orifice plate	A_o	m^2
Specific heat capacity of air	C_p	J/kgK
Length of SAH duct	L	m
Width of SAH duct	W	m
Height of SAH duct	H	m
Acceleration due to gravity	g	m/s^2
Mass flow rate of air	$\dot{m}$	Kg/s
Thermal conductivity of air	k	W/mk
Test section pressure drop	ΔP_d	N/m^2
Orifice meter pressure drop	ΔP_o	N/m^2
Useful heat gain	Q_u	W
Rise in air temperature	ΔT	˚C
Outlet air temperature	T_o	˚C
Air Inlet Temperature	T_i	˚C
Ambient temperature	T_o	˚C
Intensity of solar radiation	I	W/m^2
Mean absorber plate temperature	T_{pm}	˚C
Mean air temperature in the duct	T_{fm}	˚C
Average velocity of air	V	m/s
Wind velocity	W_V	m/s
Coefficient of discharge	C_d	-
Hydraulic diameter of duct	D_h	mm
Roughness pitch	p	mm
Roughness or ball's height	e	mm
Diameter of spherical ball	d_b	mm
Angle of attack	α	˚

Diameter of orifice	D	mm
Solar air heater	SAH	-
Cross-section	c/s	-
versus	v/s	-

Dimensionless Parameters

Name of parameter	Symbol
Relative roughness pitch	p/e
Relative roughness height	e/D_h
Spherical ball height to diameter ratio	e/d_b
Relative angle of attack	α/55
Friction factor	f
Friction factor for smooth surface	f_s
Friction factor for roughened duct	f_r
Nusselt number	Nu
Nusselt number for roughened duct	Nu_r
Prandtl number	Pr
Reynolds number	Re
Aspect ratio of collector duct	W/H

Greek symbols

Name of Parameters	Symbol	Unit
Dynamic viscosity of air	μ	N s/m^2
Air density	ρ	Kg/m^3
Density of manometric fluid	ρ_m	Kg/m^3
Angle of attack	α	°
Ratio of orifice diameter (D_2) to pipe internal diameter (D_1).	β	-
Kinematic viscosity of air	ν	m^2/s
Relative angle of attack	α/55	°
Thermal efficiency	η_{th}	%

Suffix

r	Roughened
s	Smooth
i	Inlet
o	Outlet
f	Fluid
a	Air

APPENDIX-A

Uncertainty Analysis

The experimental data recorded during investigation often differ from the actual data due to a lot of unaccountable factors while performing experiments. This deviation of the recorded data from actual data is called as uncertainty. The

uncertainty prevailing in the measurement of various parameters has been calculated following a simple procedure suggested by Klein and McClintock. The procedure for the evaluation of uncertainty has been discussed below:

Let a parameter be calculated using certain measured quantities as,

$y = y(x_1, x_2, x_3, \ldots\ldots, x_n)$

Then uncertainty in measurement of y is given as follows:

$$\delta_y = \left[\left(\frac{\delta_y}{\delta_{x_1}}\delta_{x_1}\right)^2 + \left(\frac{\delta_y}{\delta_{x_2}}\delta_{x_2}\right)^2 + \left(\frac{\delta_y}{\delta_{x_3}}\delta_{x_3}\right)^2 + \ldots\ldots\ldots + \left(\frac{\delta_y}{\delta_{x_n}}\delta_{x_n}\right)^2\right]^{0.5} \quad (1)$$

Where, $\delta_{x_1}, \delta_{x_2}, \delta_{x_3}, \ldots\ldots\ldots\ldots\delta_{x_n}$ are the possible errors in measurements of x_1, x_2, x_3 …x_n.

δ_y is absolute uncertainty and $\frac{\delta_y}{y}$ is relative uncertainty.

Uncertainty in the measurement of various parameters:

1. Area of flow, plate and orifice meter

$$\frac{\delta A_p}{A_p} = \left[\left(\frac{\delta L}{L}\right)^2 + \left(\frac{\delta W}{W}\right)^2\right]^{0.5} \quad (2)$$

Area of absorber plate (A_p):

$A = W \times L$

$$\frac{\delta A_p}{A_p} = \left[\left(\frac{1}{1200}\right)^2 + \left(\frac{0.05}{330}\right)^2\right]^{0.5}$$

$= 8.469 \times 10^{-4}$

$= 0.0008469$

$$\frac{\delta A_{flow}}{A_{flow}} = \left[\left(\frac{\delta H}{H}\right)^2 + \left(\frac{\delta W}{W}\right)^2\right]^{0.5} \quad (3)$$

Cross sectional area of air flow duct (A):

$$\frac{\delta A_c}{A_c} = \left[\left(\frac{\delta H}{H}\right)^2 + \left(\frac{\delta W}{W}\right)^2\right]^{0.5}$$

$$\frac{\delta A_c}{A_c} = \left[\left(\frac{0.05}{30}\right)^2 + \left(\frac{0.05}{330}\right)^2\right]^{0.5}$$

$= 1.67 \times 10^{-3}$

$= 0.001671$

Area of orifice meter (A_o):

$$\frac{\delta A_o}{A_o} = \left[\frac{\left(\frac{\pi D_o \times \delta D_o}{2} \right)}{\frac{\pi D_o^{\,2}}{4}} \right]^{0.5} \tag{4}$$

$$\frac{\delta A_o}{A_o} = \left[\frac{2\delta D_o}{D_o} \right]$$

$$\frac{\delta A_o}{A_o} = \left[\frac{2 \times 0.05}{38} \right]$$

$= 2.631 \times 10^{-3}$

$= 0.002631$

2. Hydraulic diameter

$$\frac{\delta D_h}{D_h} = \frac{\left[\left(\frac{\delta D_h \delta W}{W} \right)^2 + \left(\frac{\delta D_h \delta H}{H} \right)^2 \right]^{0.5}}{\left[2(W \times H)(W + H) \right]^{-1}} \tag{5}$$

$$\frac{\delta D_h}{D_h} = \frac{\left[\left(\frac{0.05 \times 0.05}{330} \right)^2 + \left(\frac{0.05 \times 0.05}{30} \right)^2 \right]^{0.5}}{\left[2(330 \times 30)(330 + 30) \right]^{-1}}$$

$= 3.731 \times 10^{-3}$

$= 0.003731$

3. Density

$$\frac{\delta \rho_a}{\rho_a} = \left[\left(\frac{\delta P_a}{P_a} \right)^2 + \left(\frac{\delta T_o}{T_o} \right)^2 \right]^{0.5} \tag{6}$$

$$\frac{\delta \rho_a}{\rho_a} = \left[\left(\frac{0.2}{101} \right)^2 + \left(\frac{0.41}{39} \right)^2 \right]^{0.5}$$

$= 0.00106$

4. Mass flow rate

$$\frac{\delta \dot{m}}{\dot{m}} = \left[\left(\frac{\delta C_d}{C_d} \right)^2 + \left(\frac{\delta A_o}{A_o} \right)^2 + \left(\frac{\delta \rho_a}{\rho_a} \right)^2 + \left(\frac{\delta \Delta P_o}{P_o} \right)^2 \right]^{0.5} \tag{7}$$

$$\frac{\delta \dot{m}}{\dot{m}} = \left[\left(\frac{0.005}{0.62} \right)^2 + (0.002631)^2 + (0.00106)^2 + \left(\frac{0.14}{354} \right)^2 \right]^{0.5}$$

$= 8.411 \text{ x } 10^{-3}$

$= 0.008411$

5. Velocity of air through test section

$$V = \frac{\dot{m}}{\rho (WH)} \tag{8}$$

$$\frac{\delta V}{V} = \left[\left(\frac{\delta \dot{m}}{\dot{m}} \right)^2 + \left(\frac{\delta \rho}{\rho} \right)^2 + \left(\frac{\delta W}{W} \right)^2 + \left(\frac{\delta H}{H} \right)^2 \right]^{0.5}$$

$$\frac{\delta V}{V} = \left[(0.008411)^2 + (0.00106)^2 + \left(\frac{0.05}{330} \right)^2 + \left(\frac{0.05}{30} \right)^2 \right]^{0.5}$$

$= 7.63 \text{ x } 10^{-3}$

$= 0.00763$

6. Reynolds Number (Re)

$$\text{Re} = \frac{\rho V D_h}{\mu} \tag{9}$$

$$\frac{\delta \text{Re}}{\text{Re}} = \left[\left(\frac{\delta V}{V} \right)^2 + \left(\frac{\delta \rho}{\rho} \right)^2 + \left(\frac{\delta D_h}{D_h} \right)^2 + \left(\frac{\delta \mu}{\mu} \right)^2 \right]^{0.5}$$

$$\frac{\delta \text{Re}}{\text{Re}} = \left[(0.00763)^2 + (0.00106)^2 + (0.003731)^2 + \left(\frac{0.002}{1.89} \right)^2 \right]^{0.5}$$

$= 8.051 \text{ x } 10^{-3}$

$= 0.008051$

7. Useful heat gain

$$\frac{\delta Q_u}{Q_u} = \left[\left(\frac{\delta \dot{m}}{\dot{m}} \right)^2 + \left(\frac{\delta C_p}{C_p} \right)^2 + \left(\frac{\delta \Delta T}{\Delta T} \right)^2 \right]^{0.5} \tag{10}$$

$$\frac{\delta Q_u}{Q_u} = \left[(0.008411)^2 + \left(\frac{1.4}{1005}\right)^2 + \left(\frac{0.68}{24.48}\right)^2 \right]^{0.5}$$

= 0.03753

8. Heat transfer co-efficient (h)

$$\frac{\delta h}{h} = \left[\left\{\frac{\delta Q}{Q}\right\}^2 + \left\{\frac{\delta A_p}{A_p}\right\}^2 + \left\{\frac{\delta (T_{pm})}{(T_{pm})}\right\}^2 \right]^{0.5} \quad (11)$$

$$\frac{\delta h}{h} = \left[\{0.03753\}^2 + \{0.0008469\}^2 + \left\{\frac{0.29}{(29.77)}\right\}^2 \right]^{0.5}$$

= 0.04865

9. Nusselt number (Nu)

$$\frac{\delta Nu}{Nu} = \left[\left\{\frac{\delta h}{h}\right\}^2 + \left\{\frac{\delta D_h}{D_h}\right\}^2 + \left\{\frac{\delta (k)}{(k)}\right\}^2 \right]^{0.5} \quad (12)$$

$$\frac{\delta Nu}{Nu} = \left[\{0.04865\}^2 + \{0.003731\}^2 + \left\{\frac{\delta (0.00001)}{(0.02652)}\right\}^2 \right]^{0.5}$$

= 0.04357

10. Friction factor (f)

$$\frac{\delta f}{f} = \left[\left\{\frac{\delta (\Delta p_d)}{(\Delta p_d)}\right\}^2 + \left\{\frac{\delta D_h}{D_h}\right\}^2 + \left\{\frac{\delta (L)}{L}\right\}^2 + \left\{\frac{\delta (V)}{V}\right\}^2 + \left\{\frac{\delta (\rho)}{\rho}\right\}^2 \right]^{0.5} \quad (13)$$

$$\frac{\delta f}{f} = \left[\left\{\frac{(0.01)}{(10)}\right\}^2 + \{0.003731\}^2 + \left\{\frac{(0.67)}{1200}\right\}^2 + \{0.00763\}^2 + \{0.00106\}^2 \right]^{0.5}$$

= 0.04871

The uncertainty analysis has been carried out for the entire set of parameter investigated within the operating range and the uncertainty variation of various parameters obtained is presented in Table 2.